JGR Oceans

RESEARCH ARTICLE
10.1029/2018JC014774

Lateral Heat Transport in the Lofoten Basin: Near-Surface Pathways and Subsurface Exchange

Johannes Dugstad[1], Ilker Fer[1], Joe LaCasce[2], Martha Sanchez de La Lama[2], and Marta Trodahl[2]

[1]Geophysical Institute and Bjerknes Centre for Climate Research, University of Bergen, Bergen, Norway, [2]Department of Geosciences, University of Oslo, Oslo, Norway

Key Points:
- Surface drifters with long residence time in the Lofoten Basin are advected over the Vøring Plateau
- Surface drifters do not capture eddies shed from the slope current off the Lofoten Islands
- Heat advection from south dominates near surface; eddy fluxes from slope dominate subsurface

Correspondence to:
J. S. Dugstad,
johannes.dugstad@uib.no

Citation:
Dugstad J., Fer, I., LaCasce, J., Sanchez de La Lama, M., & Trodahl, M. (2019). Lateral heat transport in the Lofoten Basin: Near-surface pathways and subsurface exchange. *Journal of Geophysical Research: Oceans*, *124*. https://doi.org/10.1029/2018JC014774

Received 16 NOV 2018
Accepted 14 APR 2019
Accepted article online 22 APR 2019

Abstract The Lofoten Basin in the Nordic Seas plays a central role in the Atlantic overturning circulation by acting as a reservoir for the warm and saline Atlantic Water flow toward the Arctic Ocean. The mass and heat exchange between Atlantic Water and the Lofoten Basin impacts the water mass transformations and the surface heat loss, but the processes governing this exchange are not well understood or quantified. Here we study the circulation in the Nordic Seas and the heat transport in the Lofoten Basin using a combination of Lagrangian and Eulerian methods. We analyze the trajectories of about 150 surface drifters, augmented with a set of about 47,000 surface trajectories calculated using the output from a regional numerical simulation, to investigate the drifter pathways and their exchange with the Lofoten Basin. The drifters reveal that water parcels with long residence time inside the basin contribute substantially to the heat loss and typically enter from south across the outer rim of the Vøring Plateau and, to some extent from east, from the eastern branch of the Norwegian Atlantic Current. The main contributors to the lateral heat transport to the Lofoten Basin are the near-surface heat transport by the mean flow in the southern sector of the basin and the subsurface eddy fluxes from the Lofoten Escarpment in the east.

1. Introduction

The Nordic Seas (the Norwegian, Iceland, and Greenland Seas) are a key region for the northward-flowing warm water masses from the North Atlantic Ocean toward the Arctic Ocean (Rossby et al., 2009; Segtnan et al., 2011). In this study, we focus on the Lofoten Basin (LB) of the Norwegian Sea, an area of importance for the heat transport of the northward-flowing Norwegian Atlantic Current (NwAC) (Bosse et al., 2018; Isachsen, 2015; Köhl, 2007; Raj et al., 2015; Volkov et al., 2015). At the Vøring Plateau, the NwAC splits into an eastern and western branch (Figure 1), each transporting warm water toward higher latitudes. These branches, later referred to as the "Slope Current" and the "Front Current," respectively (Orvik & Niiler, 2002), bound the LB and affect the exchange of water masses between the currents and the basin. The LB is a major heat reservoir in the Nordic Seas (Nilsen & Falck, 2006), manifested in the satellite sea surface temperature imagery (Koszalka et al., 2012), showing a warm wedge of water between the NwAC branches. Pooling of the warm Atlantic Water (AW) creates large buoyancy losses (Richards & Straneo, 2015), giving rise to convection and deep mixed layers (Bosse et al., 2018; Raj et al., 2015). Deep-reaching winter convection and vertical mixing in the western part of the LB substantially modifies the AW (Bosse et al., 2018).

The prevailing notion is that the mesoscale eddy field plays an important role in mediating the mass and heat exchange between the AW and LB. This in turn produces a substantial heat loss in the area, permitting the water masses to become denser and possibly sink as they later approach the Arctic. Even though the heat loss and convection are spread throughout the basin, the mean downwelling in the LB is localized to small segments of its eastern boundary current (the Slope Current) along steep slopes where eddies are shed (Spall, 2010). Earlier studies suggested that a significant portion of the exchange between the NwAC and the LB is a result of this eddy shedding from the Slope Current (Isachsen, 2015; Isachsen et al., 2012; Köhl, 2007; Rossby et al., 2009; Volkov et al., 2013). The Slope Current flows along steep topography off the Lofoten Escarpment, where it can reach velocities of 1 m/s (Andersson et al., 2011) and become unstable. Isachsen (2015) showed that the steep continental slope off the Lofoten-Vesterålen Islands exhibits enhanced unstable baroclinic growth rates and large velocity variability, suggesting high lateral diffusion rates. Investigating heat flux convergence, Isachsen et al. (2012) suggested that warm core eddies from the Slope

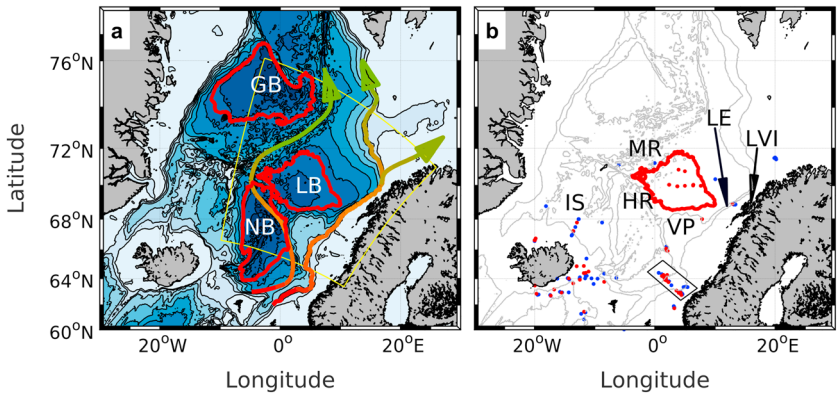

Figure 1. (a) Bathymetry of the Nordic Seas showing the typical pathways of the Norwegian Atlantic Current, indicated by arrows. Depth contours are given every 400 m. Red contours outline the three basins used in the analysis, defined by their 3,000-m isobaths. The yellow border is the domain of the ROMS 800-m model; (b) the deployment/starting positions of all 149 observed drifters analyzed in this study. Dots mark the drifters that interacted (red) or did not interact (blue) with the LB. The LB (red) and the 1,000-, 2,000-, and 3,000-m isobaths (gray) are shown. The black box encloses the Svinøy section drifters. The abbreviations which are distributed over both panels for better visibility are GB = Greenland Basin; NB = Norwegian Basin; LB = Lofoten Basin; IS = Iceland Sea; HR = Helgeland Ridge; MR = Mohn Ridge; VP = Vøring Plateau; LE = Lofoten Escarpment; LVI = Lofoten-Vesterålen Islands.

Current could transport warm water offshore. These eddies are typically anticyclonic and drift westward where the topographic depression attracts them toward the center of the LB (Köhl, 2007; Volkov et al., 2013). Based on eddy-resolving numerical models, Volkov et al. (2015) reported that the eddies are shed where the shelf topography is steepest and that they move along a cyclonic path toward the center of the basin.

In addition to the slope exchange with the basin, a feature that has gained attention is the Lofoten Basin Eddy (LBE). This quasi-permanent anticyclonic eddy in the western part of the LB (Ivanov & Korablev, 1995; Søiland & Rossby, 2013) is associated with a local maximum of sea surface height variability and eddy kinetic energy (EKE) (Köhl, 2007; Volkov et al., 2015). Evolution of the LBE core using Seaglider observations (Yu et al., 2017) showed a mean eddy radius of 18 km and an anticyclonic azimuthal peak velocity between 0.5 and 0.7 m/s at depths between 700 and 900 m. Fer et al. (2018) reported increased turbulent dissipation rates associated with large shear beneath the azimuthal velocity maximum and from subinertial energy trapped by the negative vorticity of the eddy. The LBE kinetic energy is suggested to be maintained by merging with anticyclonic eddies shed from the Slope Current (Köhl, 2007; Raj et al., 2015; Volkov et al., 2015). The heightened eddy variability is also illustrated by surface drifter data (Koszalka et al., 2011; Laurindo et al., 2017), which showed local enhancements in the horizontal distribution of lateral diffusivity in the LBE region and along the Slope Current off the Lofoten Escarpment.

The previously cited studies suggest mechanisms and pathways for the lateral heat transport into the LB; however, these are not fully understood or quantified. Here we seek to understand how the high sea surface temperatures and the large surface heat fluxes in the LB are maintained, by investigating pathways and circulation of AW and the role of advection and eddy fluxes. We analyze observations from in situ surface drifters, augmented by a set of surface trajectories computed from a 4-km horizontal grid resolution regional model of the Nordic Seas. The 4-km domain spans a large area, allowing us to estimate near-surface pathways into the LB. We assume that the surface drifters are representative of the near-surface water mass paths and exchanges. Volume-integrated heat transports for the major basins of the Nordic Seas, computed using this model, highlight the importance of the LB. We study the LB in detail, by increasing the grid resolution to 800 m, in a smaller model domain which focuses on the Lofoten region (yellow border in Figure 1a). The 800-m resolution resolves the mesoscale eddies, allowing us to estimate the relative contribution of heat transport associated with the mean flow and with the eddy fluxes.

The warm core eddies that merge with the LBE make a substantial contribution to the surface heat loss since the associated water parcels will experience long residence times in a colder environment. The typical pathways of surface drifters reaching the LB, however, suggest a broad entry of AW along the southern part of the basin instead of from the east, which would be expected from eddies shed from the Lofoten Escarpment. Our findings also emphasize the role of subsurface processes, consistent with Rossby, Ozhigin, et al. (2009)

and Rossby, Prater, and Søiland (2009), who reported a higher percentage of subsurface RAFOS floats that entered the LB from the Slope Current than for surface drifters. Thus, the eddy shedding from this region may have a stronger signature in deeper layers than near the surface.

The paper is organized as follows. The observed drifter data, the trajectories from numerical calculations, and the description of the numerical models used are presented in section 2. In section 3.1, we present integrated properties from all major basins of the Nordic Seas, using the 4-km model, to set the context and emphasize the role of the LB in the Nordic Seas. Pathways and statistics from the Lagrangian analysis are presented and discussed in section 3.2 using observed drifters and trajectories obtained from the 4-km model fields. Using the eddy-resolving 800-m model, we then concentrate on the LB and quantify the contribution of mean and eddy fluxes and of surface and subsurface signatures dominating the heat budget of the LB (section 3.3). Concluding remarks are summarized in section 4.

2. Data and Methods

2.1. Surface Drifter Data

We study the trajectories of all available surface drifters, 571 in total, that were deployed in or entered the Nordic Seas between 1991 and 31 December 2017. These data were obtained from the Global Array Drifter Program (Lumpkin et al., 2013). The GPS-tracked surface drifters are drogued at 15-m depth, with a near-surface temperature sensor at approximately 0.3 m with 0.1-K resolution. Real-time drifter data can be unevenly sampled, with a sampling frequency changing from 1 hr to, in some occasions, 1 day. Therefore, drifter positions are quality-controlled and interpolated by a kriging method to 6-hr intervals by the Atlantic Oceanographic and Meteorological Laboratory (AOML) and the National Oceanic and Atmospheric Administration (NOAA) Drifter Data Assembly Center (Lumpkin & Pazos, 2007), transmitting data of longitude/latitude, zonal/meridional velocities, and temperature. In total, the set of drifters gives approximately 140,000 days of data, spanning 30 years. We determine pathways, entry/exit positions into and out of the LB, and link the residence times inside the basin with the entry/exit positions and to each drifter's deployment location. The LB is defined as the region lying within the 3,000-m isobath (Figure 1), a contour that is approximately closed, with one exception being a 28-km-long segment in the southwest toward the Norwegian Sea between the coordinates [0.78°W, 69.3°N] and [0.84°W, 69.5°N]. We manually closed this segment. Since our main interest is to investigate the pathways of warm AW, we exclude the drifters that were deployed north of the LB or which never reached the latitudes of the LB.

Out of a total of 571 drifters, we selected 149 drifters for analysis. Of the rejected drifters, 128 lost their drogue upon deployment, 21 lacked drogue information, 66 were deployed north of the LB, and 207 did not reach the LB latitudes. Of the latter 207, 81 drifters ran aground near Iceland or along the western coast of Norway, and 126 stopped transmitting good-quality data (three from poor battery performance and the remaining 123 because of rough seas).

Drifter mortality is a problem in the Nordic Seas. The drifter population experiences a nearly exponential decay in time after deployment (Koszalka et al., 2012). The subset of drifters selected in this study has an e-folding time scale of 190 days, less than half the value given in Lumpkin et al. (2012). A typical drifter propagating northward from areas around Iceland travels a distance of approximately 900 km to reach the center of the LB, in more than 100 days with an average speed of 10 cm/s. Drifter mortality therefore complicates the estimation of drifter interaction with the LB.

2.2. Trajectories From a Numerical Model

The observed drifters are deployed geographically nonuniform, in selected key sections and locations, and our data selection further reduces the number of drifters studied. In such a scarce and nonuniform data set, the statistics of the Lagrangian observations are limited and biased (Davis, 1991). Therefore, we generate a set of surface trajectories of water parcels forced by a numerical model of the Nordic Seas with 4-km grid resolution (the model is described in section 2.3). In the following, we refer to these trajectories as "synthetic drifters." The synthetic drifters disperse in a quantifiable manner and therefore permit the investigation of a number of trajectories several orders of magnitude larger than for observed drifters. This improves the statistical significance. Furthermore, we can conduct controlled and uniformly distributed releases to reduce the bias.

The synthetic drifter data set consists of approximately 115,000 particles deployed in the Nordic Seas. The seeding is in uniform groups, inside the box given by 64–78°N and 15°W–15°E, with $40 \times 40 = 1,600$

drifters. The groups of 1,600 drifters are deployed at the same location, every eighth day over a period of 1.5 years. The daily velocity fields from the 4-km model (see section 2.3 for details) are used to advect the drifters to new positions after interpolating to 1-hourly time steps, by using a fourth-order Runge Kutta routine. The trajectories are then stored at 6-hr intervals. Assuming that all information about the flow is contained in the model velocity fields, we do not add explicit diffusion in the simulations. The simulations for each group are run for 1 year; hence, drifter lifetimes are limited to 1 year. The model applies absorbing boundary conditions, that is, a drifter which runs aground is terminated. The model domain is large, and the synthetic drifters do not reach the model's open ocean boundary during their lifetime. The calculations are 2-D; hence, no vertical exchange is allowed. To be consistent with observations, we exclude all drifters deployed north of the LB or those that do not reach the latitudes of the LB, giving approximately 47,000 trajectories for analysis.

2.3. Eulerian Calculations

The Eulerian calculations are based on the Regional Ocean Modeling System (ROMS) simulations. ROMS is a primitive equation model with free surface and terrain-following vertical coordinates and is horizontally gridded as a staggered C-grid (Haidvogel et al., 2008; Shchepetkin & McWilliams, 2005, 2009). Results from two model domains are analyzed. Our relatively coarse horizontal resolution (4 km) model covers all the Nordic Seas (see Figure 2 in Trodahl & Isachsen, 2018, for the full domain) and allows us to compare different basins. A smaller domain with 800-m resolution was constructed to provide eddy-resolving output focused on the LB. Both models consist of 35 vertical layers and are stored as daily averages. This temporal resolution is sufficient to resolve the mesoscale and submesoscale processes (Isachsen, 2015; Trodahl & Isachsen, 2018). The models also span similar time periods. The 4-km model covers from 1993 to 2005, while the 800-m model duration is 1 year shorter, from 1993 to 2004, because of limited computational resources.

The two simulations are forced identically and share the same model setup. A fourth-order-centered scheme is used for vertical advection and a third-order upwind scheme for horizontal tracer and momentum advection. The upwind advection scheme implicitly includes some biharmonic diffusion. No explicit horizontal eddy viscosity or diffusion is applied. Small-scale vertical mixing is parameterized by the k-ϵ version of the General Length Scale scheme (Umlauf & Burchard, 2003; Warner et al., 2005). The open lateral boundaries are relaxed toward monthly fields from the Global Forecast Ocean Assimilation Model (MacLachlan et al., 2015), and the atmospheric forcing is provided by 6-hourly fields from the ERA-interim atmospheric reanalysis (Uppala et al., 2005). Runoff from primary rivers are supplied by monthly climatologies. The 4-km model was validated and analyzed in Trodahl and Isachsen (2018).

Due to the larger model domain, the 4-km simulation requires a longer spin-up time than the 800-m simulation. Taking this into account and requiring the same time span for consistency, we analyze the 8-year period from 1 January 1997 to 1 January 2005 for the 4-km model and from 1 January 1996 to 1 January 2004 for the 800-m model.

Using the 4-km model, we compute the mixed layer depth (MLD) in the LB, the Norwegian Basin, and the Greenland Basin (see Figure 1a for their locations). The MLD is obtained as the depth at which the density increases from its surface value by 0.01 kg/m^3 (Peralta-Ferriz & Woodgate, 2015; Toole et al., 2010). The maximum MLD in each grid point is the maximum value over the simulation time span. In addition, we integrate the net surface heat flux over each basin, using the annual averaged fluxes in the corresponding 8-year analysis period. We compare this to the net heat transport into each basin computed around the closed basin contours using

$$\mathrm{HT} = \rho C_p \int_H \int_S \langle \mathbf{U}T \rangle \cdot \mathbf{n} \, ds \, dh. \tag{1}$$

Here ρ is the density of seawater, C_p is the specific heat capacity, $\mathbf{U} = (u, v)$ is the horizontal velocity vector, T is the temperature, ds and dh are length elements around the basin contour of integration and in the vertical, respectively, and $\mathbf{n}$ is the unit normal vector pointing into the basin. Thus, positive values indicate heat transport into the basin. The vector $\langle \mathbf{U}T \rangle$ is time averaged in the same way as the surface heat flux, indicated by the angle brackets. Normally, the heat transport should be computed relative to some reference temperature T_{ref}. However, note that we integrate over the entire water column and that the basin contours are closed. Thus, we operate with closed volumes, and because of mass conservation, the term associated with T_{ref} will not contribute to the integral. Since the currents in the Nordic Seas are, to a large extent,

Table 1
Surface Area, Integrated VB, Integrated HT, SHL (Temporal Mean ± Standard Deviation), Average Maximum MLD, and Surface EKE for the LB, the NB, and the GB for the 4-km Model

Basin	Area (10^5 km^2)	VB (Sv)	HT (TW)	SHL (TW)	Max. MLD (m)	EKE (cm^2/s^2)
LB	1.1	0.0	7.3 ± 2.7	5.2 ± 1.2	480	64.2 (330.0)
GB	1.2	0.3	0.6 ± 0.8	2.0 ± 0.8	580	44.3
NB	1.7	−0.3	2.6 ± 2.1	1.4 ± 1.0	190	38.7

Note. The EKE in the LB from the 800-m model is also given in brackets. Averaging is over the full 8-year period (1 January 1997 to 1 January 2005). Standard deviations are computed from the year-to-year variability over the analyzed period. 1 TW = 10^{12} W; 1 Sv = 10^6 m^3/s. VB = Volume transport Balance; HT = Heat Transport; SHL = Surface Heat Loss; MLD = mixed layer depth; EKE = eddy kinetic energy; LB = Lofoten Basin; GB = Greenland Basin; NB = Norwegian Basin.

topographically steered (Isachsen et al., 2003; Nøst & Isachsen, 2003), the basin contours are defined by the 3,000-m isobaths on the ROMS model grid, similar to the LB definition applied for the drifter analysis. Since the velocity variables are located on the borders of the staggered grid cells, we define the points on the basin contours to be located in the corners of these grid cells, the so-called psi points. We further define the vectors between the psi points on the basin contours to be purely horizontal or vertical, thus avoiding interpolation of velocity when integrating the heat transport around the contour.

For a more detailed analysis with focus in the LB, we take advantage of the eddy-resolving 800-m resolution model results. Calculations of surface heat flux and the heat transport in the LB are done identically to the 4-km model. Additionally, to quantify the relative contribution of the mean and eddy components, we apply Reynolds averaging of the daily-mean fields

$$\langle uT\rangle = \langle u\rangle\langle T\rangle + \langle u'T'\rangle. \tag{2}$$

A similar equation is applied on the v velocities. Here $u = \langle u\rangle + u'$ and $T = \langle T\rangle + T'$, where $\langle u\rangle$ and $\langle T\rangle$ are time averages and u' and T' are the corresponding perturbation fields. EKE density is computed as $\frac{1}{2}\left(\langle u'^2\rangle + \langle v'^2\rangle\right)$. To exclude the seasonal variability in the computation of the eddy fluxes, the averages are calculated over four periods during a year, that is January–March, April–June, July–September, and October–December. Annual averages are then obtained by averaging over the four values each year between 1 January 1996 and 1 January 2004 or for some scenarios over the entire 8-year period. We refer to these averages as annual averages or 8-year averages, respectively, when discussing the 800-m model in the text.

3. Results and Discussion

3.1. The Importance of the LB

The surface area of LB covers approximately one fifth of the Nordic Seas but is responsible for approximately one third of the total buoyancy loss in the region (Richards & Straneo, 2015). In the western part of the LB, Bosse et al. (2018) estimated a temperature decrease in AW by about 2.6 °C on its way northward, a more rapid cooling than any other region in the Nordic Seas. Using hydrographic measurements, Raj et al. (2015) obtained winter MLDs of 560 m in the LB, one of the largest values in the Nordic Seas. This deep thermal convection together with large buoyancy losses to the atmosphere implies pooling of warm water in the LB.

In Table 1, we contrast the integrated properties in the three main basins, the LB, the Norwegian Basin, and the Greenland Basin, using the 4-km model outputs. The heat transports integrated over the closed basin volume is largest into the LB (Figure 2), verifying that the LB is the most important area for the northward-flowing AW. The surface heat loss averaged over the period 1997–2005 reveals that among the major basins in the Nordic Seas, the LB accounts for approximately two thirds of the surface heat loss. More heat is transported into the LB and the Norwegian Basin than lost at surface, while it is the opposite for the Greenland Basin. Similar imbalances were inferred from observations in Segtnan et al. (2011). The heat imbalances imply warming of the LB and the Norwegian Basin, whereas the imbalance in the Greenland Basin is not significantly different than zero. Annual averages of temperature, volume averaged in each basin, show a small increase in the LB and the Norwegian Basin associated with these imbalances, while the Greenland Basin stays at approximately the same temperature. Maximum MLD in the LB is large and

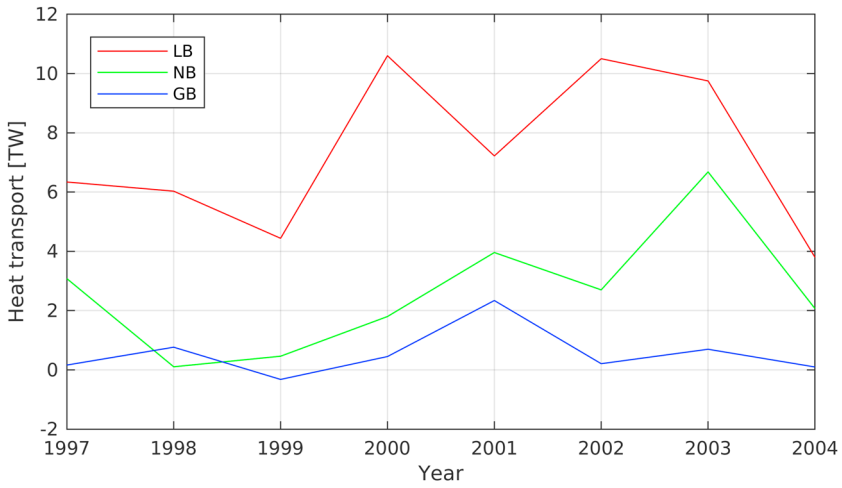

Figure 2. Integrated net heat transport for the Lofoten Basin (LB), Norwegian Basin (NB), and Greenland Basin (GB) for each year during the period 1 January 1997 to 1 January 2005. Time average values and standard deviations are given in Table 1.

comparable with the Greenland Basin (Table 1). While the Greenland Basin is recognized as a high-latitude deep and intermediate convection region (Rudels & Quadfasel, 1991), where brine rejection from sea ice formation can be important, the deep MLD in the LB is from thermal convection and cooling of the warm AW (Søiland & Rossby, 2013). In summary, the LB stands out in the Nordic Seas with large net heat transport and surface heat fluxes, giving deep MLDs.

3.2. Pathways

3.2.1. Observed Drifters

Drifter density maps are computed as the number of drifters entering defined rectangular bins in longitude and latitude. The so-called "density maps" show the distribution of drifters in the domain. In the density maps extracted from the observed drifter trajectories, the Slope Current stands out (Figure 3a) and dominates over the Front Current. Among the 149 drifters studied, 82 followed the pathway with the Slope Current, not interacting with the LB at all or passing by the southeastern rim of the LB. The observational data are biased, as a large number of drifters were deployed in the Svinøy section (black box in Figure 1b) and on the slope off the Lofoten-Vesterålen islands. However, we identified approximately 50 drifters deployed north or south of Iceland, 30 of which ended up to the east of the LB while 10 drifters propagated toward the western boundary of the LB. The remaining drifters stayed over the Helgeland Ridge (the topographic feature between the NB and LB) or entered the LB from south. Drifters deployed close to Iceland thus have a main route eastward toward the Svinøy section before turning north, in agreement with Orvik and Niiler (2002). In fact, we observed only four drifters that followed the Front Current along the Mohn Ridge northward toward Fram Strait.

The pathways of the drifters entering the LB are analyzed separately. The density of the trajectories of 46 drifters that entered the LB shows a broad entry region in the southern sector (Figure 3b).

In order to relate the residence time in the basin to the drifter entry and exit locations, we unwrap the LB contour and calculate the histograms binned in residence time and distance around the basin (Figure 4), that is, the percentage of drifters with a range of residence time entering (or exiting) at different segments around the LB contour is shown. The unwrapped LB contour starts from the northeastern corner (black cross in Figure 3c), progressing counterclockwise. The colored segments at the bottom of Figure 4 correspond to the same colored segments around the basin contour in Figure 3, starting with the red segment at 0 and following the basin counterclockwise to the end of the green segment at approximately 2,000 km.

A drifter can cross the LB boundary multiple times, giving more crossings for residence time analysis than the number of drifters we investigate. The drifters enter and exit the basin mainly in the south and east (Figures 4a and 4b). However, the majority of drifters experience short residence time inside the basin. We measure the residence time as the length of each stretch of record when a drifter was in the basin. The mean residence time inside the basin averaged over all drifter entries is 10 days. If we use the longest retention

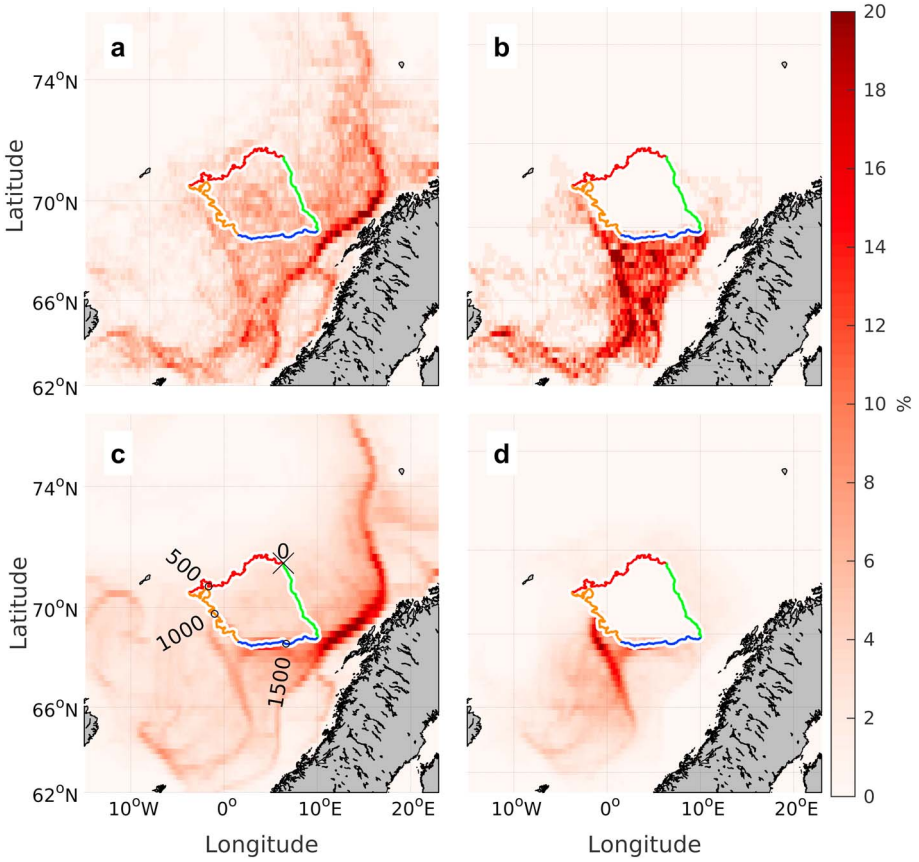

Figure 3. Density maps obtained from (a,b) the observed drifters and from (c,d) the synthetic drifters. Left panels show density maps of all drifters studied, 149 for (a) and 47,226 for (c). Right panels show density maps of drifters that interacted with the Lofoten Basin, 46 for (b) and 12,064 for (d). These are shown from deployment location until the first entry to the basin for each drifter. Color bar shows the percentage of drifters that was observed inside each bin relative to the number of drifters analyzed (listed above). Bin sizes are 0.25° × 0.25°. The white-bordered contour marks the Lofoten Basin with colors indicating the northern (red), western (orange), southern (blue), and the eastern (green) segments. For later reference, the basin contour in (c) is marked at 500-km intervals starting from the northeastern corner (black cross).

period for each drifter with multiple crossings of the basin perimeter, we obtain a mean residence time of 20 days. The hot spot for entering/exiting drifters in the southeast between 1,450 and 1,750 km accounts for approximately 40% of the drifter entries, but given their short residence time, the drifters exit before the associated water parcels are able to transfer heat to the basin. We observed seven drifters with at least one crossing into the LB with a residence time longer than 50 days (15% of the drifters that entered the LB). Their trajectories are shown in Figure 5b, together with the analogous trajectories for the drifters staying inside the basin between 15 and 50 days (12 drifters; Figure 5a).

The observed trajectories with longer residence time in the basin are not clearly linked with eddy shedding from the Slope Current. Figure 5a shows trajectories with orbital motion near and north of the steep slope between the Slope Current and the basin. These may be indicative of the eddy shedding from the unstable boundary current. Based on their relatively short residence times and the observation that they do not propagate far into the basin, their contribution to the large LB heat loss must be limited. The drifters with residence time longer than 50 days (Figure 5b) advect from south and enter the basin mainly across the southern and western segments of the LB. Observational evidence of contribution from the Slope Current into the basin is scarce. We observe one occurrence of a trajectory from slope to basin, but mainly the drifters either follow the Front Current to enter the basin in the southwest or enter the basin from south after crossing the Vøring Plateau. The drifters mainly propagate toward the basin with a meandering motion. Although the drifter observations are limited and inconclusive, they are indicative of the preferred locations of entry and exit

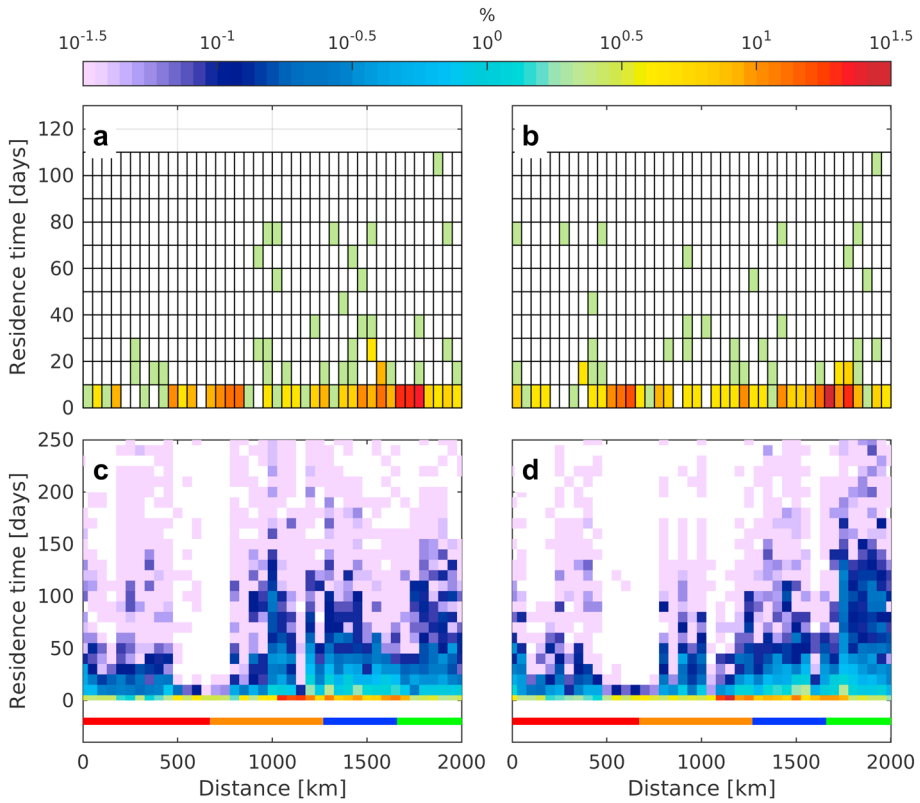

Figure 4. Histogram linking the drifter residence times inside the basin to (a,c) entry and (b,d) exit locations on the unwrapped LB contour for (a,b) observed and (c,d) synthetic drifters. Colored line at the bottom of (c) and (d) shows the unwrapped LB contour with the corresponding colors in Figure 3 for the north, west, south, and east segments. The percentage of entries/exits relative to the number of drifters interacting with the basin (46 for a and b and 12,064 for c and d) are color coded on logarithmic scale. Bins are 50 km × 10 days. Note that a drifter may cross the LB boundary several times. LB = Lofoten Basin.

into the LB and highlight the striking difference in pathways taken by the two subsets with short and long residence times in the LB. We turn to synthetic drifters to increase the statistical confidence in this finding.

3.2.2. Synthetic Drifters

The synthetic drifters obtained from the 4-km model fields were subjected to a data selection similar to that applied to the observed drifters (section 2.2), resulting in 59,112 synthetic surface drifter trajectories that were deployed south of the LB. We further removed 5,118 trajectories from drifters which ran aground before they reached the LB. Of the remaining drifters, 6,768 were deployed within the LB contour, while 12,064 were deployed outside but entered the LB at a later time. Thus, $12,064/(59,112 - 5,118 - 6,768) = 26\%$ of the drifters deployed outside the LB interacted with the basin. This is comparable to $46/149 = 31\%$ obtained for the observed drifters and suggests some confidence in the synthetic drifters. The smaller value may be because of the setup of the experiments: The synthetic drifters are deployed on a uniform grid (section 2.2) to obtain homogeneous statistics and to avoid spurious and biased representation of the flow because of geographical sampling variations (Davis, 1991), whereas the in situ drifters are deployed in key sections and locations.

The density plots of synthetic drifters (Figures 3c and 3d), subsampled similar to observations, show similarities with the observed drifter densities (Figures 3a and 3b). The Slope Current is pronounced, the drifters mainly approach from the south toward the southern LB boundary, and the Front Current densities are the strongest along the outer rim of the Vøring Plateau. The continuation toward the Mohn Ridge, however, is weak. Instead, the connection toward the Slope Current along the Vøring Plateau is stronger than previously thought.

Residence time analysis of these synthetic drifters can be compared to the observed drifters (Figure 4). In agreement with the observations, most synthetic drifters experience short periods inside the basin, and the

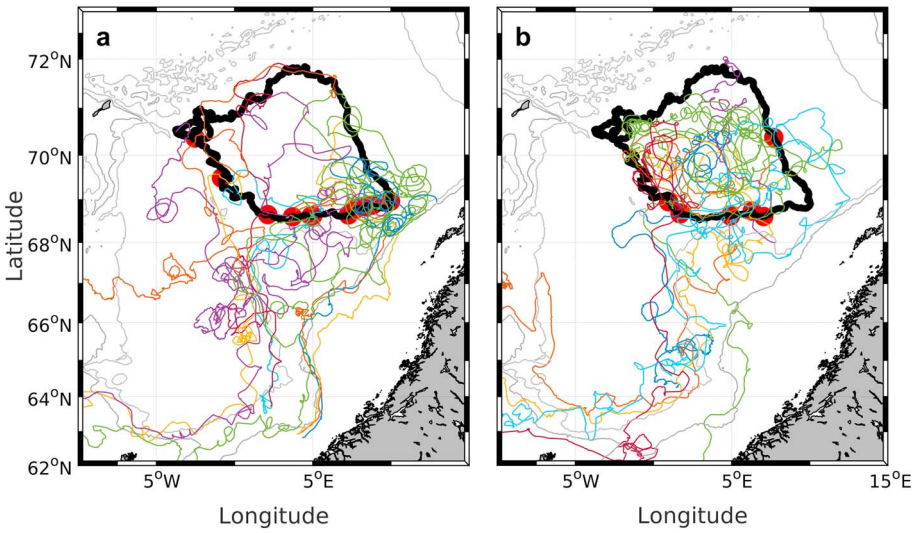

Figure 5. Drifter trajectories for (a) the 12 drifters staying inside the basin between 15 and 50 days and (b) for the seven drifters staying inside the basin for more than 50 days. The red dots mark the first entry position for each drifter into the basin. Only trajectories from deployment location until the last exit from the Lofoten Basin are shown. The 1,000- and 2,000-m isobaths are shown in gray.

associated heat loss must therefore be limited. The mean residence time for all entries into the basin is about 15 days, 5 days more than the observed drifters. The mean residence time for the longest consecutive period inside the basin for all drifters is 45 days, that is, a factor of two more than the observed drifters. The distribution of the retention periods for the synthetic drifters is highly skewed (not shown), relative to the observations (skewness of 2.2 vs. 1.6) with a longest residence time in the basin for the synthetic drifters of 363 days, 260 days longer than the observed drifters. Such long retention periods will not be captured by the observed drifters with much shorter lifetime because of mortality (from batteries and storms, section 2.1). The majority of the synthetic drifters (85%) has a longest residence time shorter than 103 days. The mean residence time of this set of synthetic drifters is 22 days, which is similar to the observations. Thus, the long residence time of synthetic drifters is mainly skewed by a small subset of drifters trapped in the LB. The synthetic drifters with a residence time longer than 50 days enter the basin mainly in the south/southwest or east (537 in north, 1,008 in west, 713 in south, and 739 in east). In the west, the entries are dominant along the southernmost part of the segment. The exit positions are mainly oriented toward the eastern part of the basin.

The large surface heat loss in the basin is expected to reduce the temperature of the synthetic drifters with prolonged periods in the basin. Using the temperature fields of the synthetic drifters, the temperature change between the entry and exit is analyzed. However, due to the seasonal cycle, the drifters can experience both warming (during summer, not shown) and cooling (during winter). Since the cooling is enhanced during winter, we focus on drifters entering the basin during these months and investigate how the temperature loss is related to residence time in the basin. We restrict the analysis to one single winter month (to reduce temporal variations due to seasonal changes). For the same reason, we do not study residence times longer than 100 days. The temperature loss is computed by calculating the difference $-(T_{\text{exit}} - T_{\text{entry}})$, between temperatures at the exit and entry times. November (3,386 crossings), December (2,742 crossings), and January (2,459 crossings) months are analyzed to test the sensitivity. Each subset shows a similar pattern and variability (not shown). We focus on November, because it has the most number of trajectories and it is followed by a long winter season (a residence time of 90 days experiences the entire winter). The cooling in winter is positively correlated ($r^2 = 0.34$) with the residence time (Figure 6a), likely facilitated by the retention induced by eddies, and shows approximately a linear increase with increasing residence time. Generally, strong winter surface heat losses in the basin can thereby impact transformation of water parcels with long residence time in the basin.

The temperature loss experienced by water parcels shows geographical variations related to the entry segments (Figure 6a). Synthetic drifters which entered the basin in November are subsampled into those with

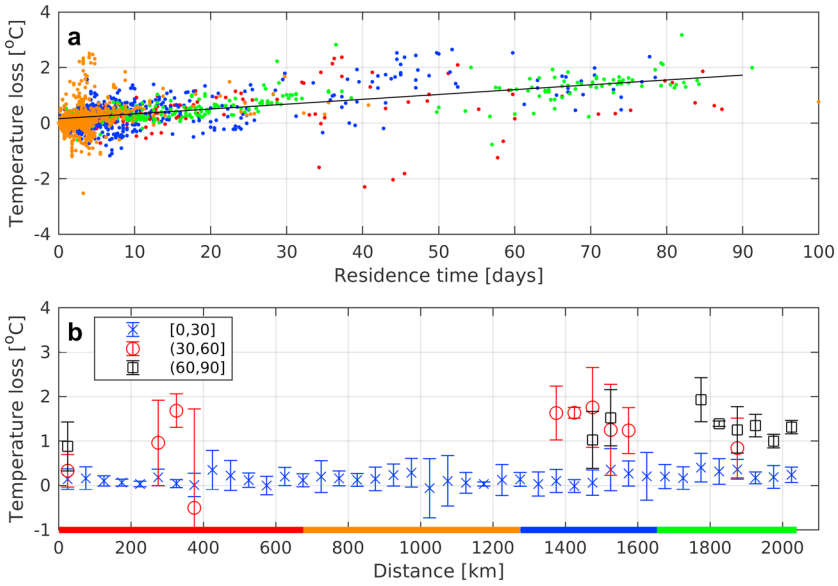

Figure 6. (a) Temperature loss variability with residence time for synthetic drifters entering the basin in November. The temperature loss is that experienced by a water parcel from entry to exit. Colored dots identify the segment of entry. A linear fit is also shown (squared linear correlation coefficient is $r^2 = 0.34$); (b) temperature loss versus entry position into the basin averaged in bin sizes of 50 km along the unwrapped basin contour. All temperature loss data of crossings from drifters going into the Lofoten Basin in the specified bin is averaged, and error bars are one standard deviation. Results are shown for drifters with a residence time between 0 and 30 days, between 30 and 60 days, and between 60 and 90 days. A bin with less than 3 data points is excluded. The colored line in the bottom marks the northern (red), western (orange), southern (blue), and the eastern (green) segments of the Lofoten Basin boundary.

residence time between 0 and 30 days, between 30 and 60 days, and between 60 and 90 days. We obtain 3,200, 96, and 88 crossings into the basin associated with these groups, respectively. The largest temperature losses, which are mainly experienced for water parcels with a residence time between 30 and 90 days, most frequently enter the basin in the south and east, indicating a large contribution to the LB heat loss from these regions (Figure 6b). Each data point is an average over all temperature data measured in horizontal bins of 50 km. An average is excluded if the number of data points inside a bin is less than 3. The averaged temperature loss taken over the southern and eastern segments were 1.4 and 0.9 °C, respectively, for drifters with residence time between 30 and 60 days and 1.3 and 1.4 ° C between 60 and 90 days. Even though the temperature losses are larger for drifters entering the basin in the south compared to east, both quantities are significant, and the synthetic drifters suggest that the heat transport across both the southern and the eastern boundaries of the LB is the largest contributors to the heat budget of the LB at surface.

3.3. Eulerian Analysis—The Role of Subsurface Processes

Using near-surface Lagrangian trajectory analysis of observed drifters, we showed that the AW enters the LB across a broad sector in the south. The water parcels associated with this flow experience the longest residence times in the basin, hence the largest heat loss in winter. Synthetic surface drifters additionally show a contribution from the east, which is supported by the earlier literature (Isachsen et al., 2012; Köhl, 2007; Raj et al., 2016). Overall, the percentage of drifters that interact with the LB (31% for the observed and 26% for the synthetic drifters) is significant but implies that a larger percentage of drifters propagates along the slope and around the rim of the basin and does not enter the LB. Furthermore, the drifters entering the LB typically have short residence times, hence experience a limited heat loss. The Slope Current carries the majority of drifters. This suggests that eddies from the Slope Current may be subsurface lenses instead of surface intensified eddies (Rossby, Prater, & Søiland, 2009), facilitating a substantial deeper interaction between AW and the LB (Rossby, Ozhigin, et al., 2009). Vertical motion might occur in certain regions due to deep MLDs. The (2-D) surface drifters will remain at surface and cannot sink, hence cannot capture the subsurface exchange. With the Eulerian fields, however, we can investigate the vertical distribution of heat fluxes and quantify the different contributions to the LB heat budget along the basin contour and in the water column.

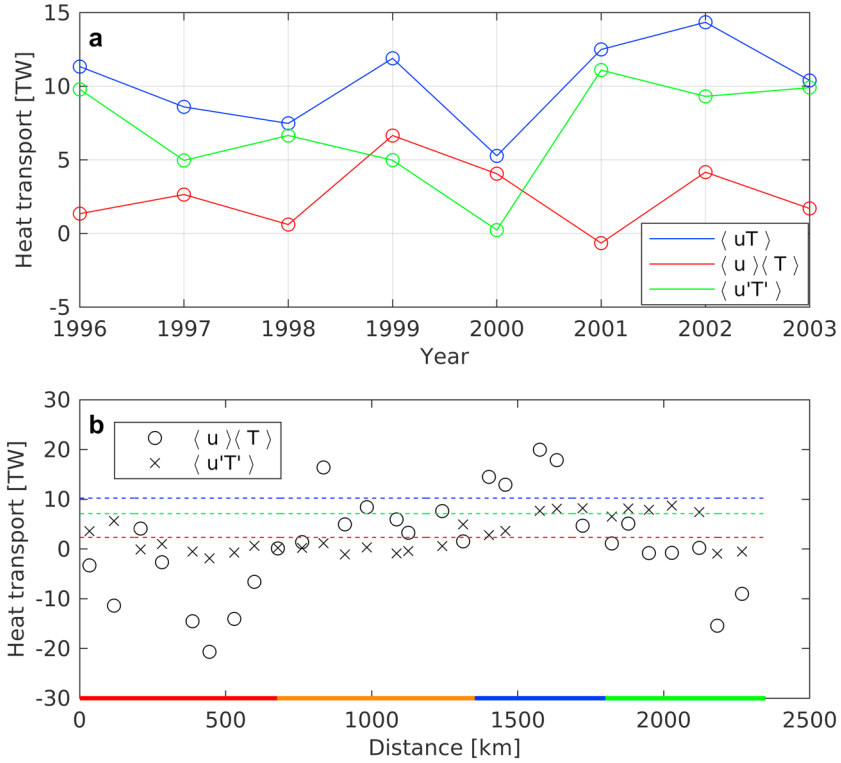

Figure 7. (a) Annual-averaged integrated heat transport around the LB for each year during the period 1 January 1996 to 1 January 2004. Total heat transport is shown in blue, while the mean heat transport and the eddy transport are shown in red/green, respectively; (b) time-averaged heat transport over 8 years from 1 January 1996 to 1 January 2004 along the unwrapped LB contour. Dashed lines are the 8-year averaged net heat transports into the basin. The colors correspond to the total, the mean, and the eddy contribution and are the same as in (a). Red, orange, blue, and green lines at the bottom identify segments of the unwrapped LB contour. LB = Lofoten Basin.

We use the eddy-resolving 800-m resolution ROMS model to investigate the net heat transport into the LB and quantify the mean and eddy contributions. As a comparison, the surface EKE averaged over the basin and over time between 1 January 1996 and 1 January 2004 is 330 cm^2/s^2, about 5 times larger than the corresponding number from the 4-km model (Table 1). The volume transport into the LB is balanced as in the 4-km model. Heat transport is computed by integrating around the closed LB contour over the entire water column, as in the 4-km model (equation (1)). Applying Reynolds averaging (equation (2)), we split the integral into a mean and an eddy component. In practice, we obtain the eddy flux, $\langle u' T' \rangle$, as the residual of the total heat transport (equation (1)) and the mean heat flux $\langle u \rangle \langle T \rangle$ (here only expressed for u), where averaging is over 1 year, after following the procedure described in the end of section 2.3. Annual total heat transports from the 800-m model (Figure 7a) are 1 to 5 TW (1 TW = 10^{12} W) larger than the LB heat transport calculations from the 4-km model (Figure 2). The 8-year average of approximately 10 TW can be compared to the ocean heat convergence of 119 TW computed by Segtnan et al. (2011) but over an area about 10 times larger than our LB area. Integrated around this closed volume, the net heat transport is mainly dominated by eddy fluxes.

We wish to describe the variability of the mean and eddy fluxes in the vertical, in the curtain of water column around the basin contour. This, however, needs to ensure the net volume transport over the averaging length is zero. In order to identify the locations along the basin contour where the eddy fluxes and the mean flow make the largest contributions to the increase of heat content inside the LB, we estimate the net heat transport through defined segment lengths of the basin contour by the following procedure. Starting from the northeast edge of the LB contour, as earlier, we integrate the volume transport first over the entire depth and then counterclockwise along the LB contour over a segment length, until the net volume transport becomes smaller than a set threshold. Below this threshold, set to 0.02 Sv, we consider the volume transport to be balanced. We integrate the heat transport over depth and along this segment and assign the result to the midpoint of the defined segment along the basin contour. This procedure is repeated by moving 2 km

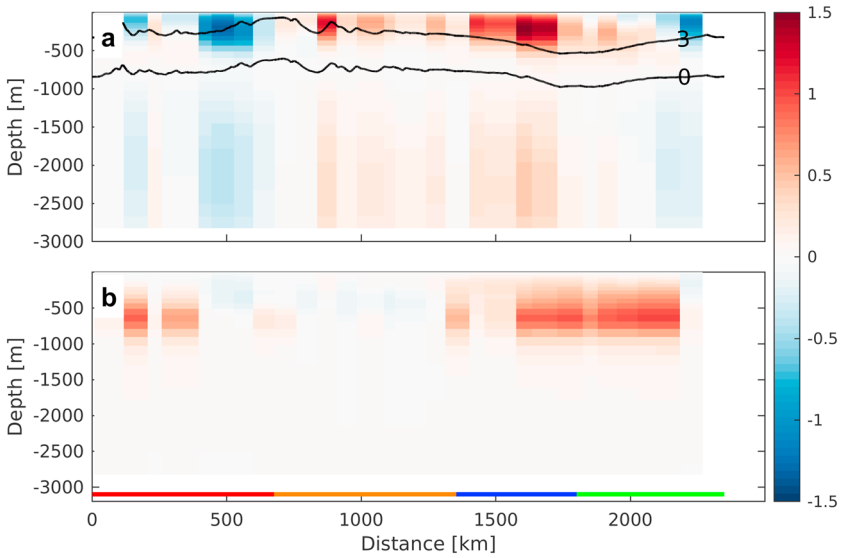

Figure 8. Vertical distribution of layer-integrated heat transport along segments with balanced volume transport for the (a) mean flow and for the (b) eddy fluxes, averaged in 80-km bins. The time averaging is similar to Figure 7b. Color bars show the heat transport in TW. Red, orange, blue, and green lines at the bottom identify the segments of the unwrapped Lofoten Basin contour. In (a), the black curves show temperature contours for 0 and 3 °C along the basin boundary.

counterclockwise along the basin contour and integrating along a new segment with balanced volume transport. The heat transports are then averaged in 80-km bins along the basin contour.

Alternatively, if one uses the volume average temperature in the LB as the reference temperature, heat transport can be calculated using arbitrary segment lengths without the requirement of zero net volume transport (Lee et al., 2004). However, the heat transport may be sensitive to the choice of the segment length. Constraining the segment lengths with zero net volume transport has the advantage that it defines the segments around the basin contour.

For this calculation, we time average between 1 January 1996 to 1 January 2004 (section 2.3). We require a minimum segment length of 200 km. The average segment length with balanced volume transport is 940 km, approximately two fifths of the length of the basin contour. We assume that the large amount of segments obtained, 1,413 in total, will be representative of where the heat fluxes enter the basin. Distribution of the time-averaged heat fluxes along the LB contour highlights where the mean or the eddy components dominate (Figure 7b). The depth-integrated heat transport indicates substantial heat into the basin as a mean flow in the southern sector (1,400–1,600 km) and of comparable magnitude transported out of the basin in the north (400–600 km). As expected, the heat associated with eddy fluxes are important in the east/northeast.

The vertical distribution of heat transport in the water column along the LB contour is calculated over the same segments with balanced volumed transport, but vertical integration is over each layer instead of the entire depth (Figure 8). The time averaging is similar to Figure 7b. The contributions of the mean flow and the eddy fluxes are presented separately. The mean flow advecting heat to the LB from the south (blue segment, 1,300–1,700 km) appears to be a near-surface feature, while the eddy fluxes supplying heat into the basin from the southeast/east/northeast are centered at approximately 700-m depth.

The heat transport, integrated around the basin and the entire depth (Figure 7a), is dominated by eddy fluxes in agreement with the earlier literature (Isachsen, 2015; Köhl, 2007; Koszalka et al., 2011). Along the LB contour, the mean heat flux shows a large variability (Figures 7b and 8) and give the largest contribution to heat input to the LB in the west and south, while the eddy fluxes dominate in the east and north. The large heat input to the LB in the south (Figures 7b and 8a) is supported by the surface drifters which showed a slab-like advective inflow to the LB in this region. These drifters entering from the south experience long residence time and significant temperature loss in the basin. Thus, the heat input in the south computed from the model is likely to contribute to the surface heat loss in the basin. Between about 600- and 800-m depth, the heat flux associated with the mean flow vanishes where the temperature of the inflow is approximately zero. At the same levels, the eddy fluxes dominate. The eddy fluxes supply heat to the LB deeper

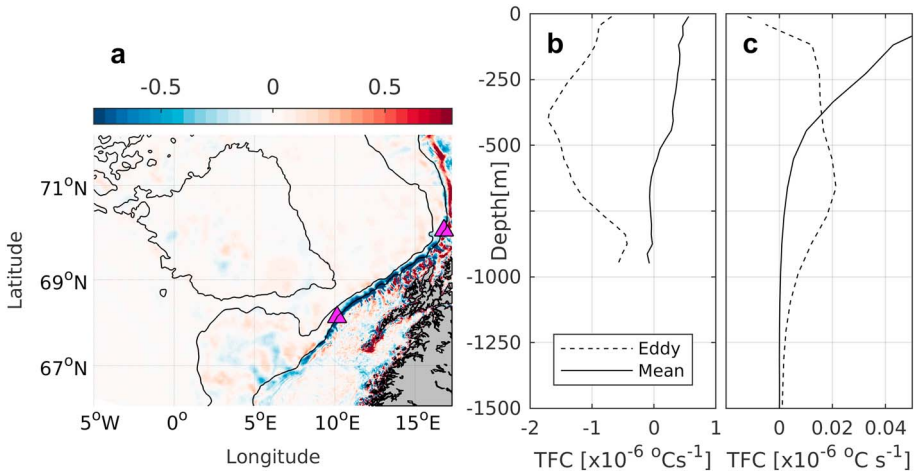

Figure 9. (a) Eddy temperature flux convergence (TFC) averaged over depth. The 1,000- and 2,000-m isobaths together with the Lofoten Basin are shown in black. Color bar shows the TFC in $10^{-6}\times$ °C/s. Triangles on the 1,000-m isobath define the segment over which the vertical profiles of mean and eddy fluxes shown in (b) are averaged. Average profiles of eddy and mean TFC are calculated over (b) the 1,000-m isobath off the Lofoten Escarpment and (c) the Lofoten Basin. Note we only show the upper 1,500 m in (c) as the fluxes vanish deeper in the water column. The time averaging is done for the period 1 January 1996 to 1 January 2004 (similar to Figures 7b and 8) for all panels.

in the water column at approximately 700 m and are not captured by surface drifters, possibly explaining why only 5% (6%) of the observed (synthetic) surface drifters stayed inside the LB more than 50 days. This is consistent with the observations of Poulain et al. (1996) and with Rossby, Prater, and Søiland (2009) who discussed the different behavior of surface drifters and RAFOS floats and found that the fraction of RAFOS floats ejected from the Slope Current toward the LB was larger than for the surface drifters. The findings are also consistent with Volkov et al. (2013) who reported differences between the eddy propagation pattern in the LB (westward and cyclonic propagation) affected by the deep currents and surface drifter trajectories. The heat from eddy fluxes between 500- and 1,000-m depth are therefore likely to give large contributions to the LB heat budget.

The results in Figures 7b and 8 are not based on closed integrals and must be interpreted with caution regarding the net heat transport. Also, they do not reveal information about the residence time in the basin. However, both the advective flux in the upper layers in the south and the eddy fluxes around 700-m depth in the east are supported by Lagrangian studies. Water parcels bringing heat into the basin at these locations also interact significantly with the basin and contribute to the heat loss. The mean heat fluxes centered around 1,500 km that advect about 1.5 TW heat into the basin are larger than the eddy fluxes of ~1 TW at 700-m depth. Since the eddy fluxes are important to close the LB heat budget (Isachsen, 2015; Isachsen et al., 2012; Köhl, 2007; Richards & Straneo, 2015; Spall, 2010; Volkov et al., 2015), our estimate of the mean heat flux from the south implies a substantial advective heat contribution.

An analysis of the temperature flux convergence (TFC) supports the inferences from the mean and eddy fluxes discussed above. We compute the negative of divergence such that a positive value indicates convergence of temperature, that is, heating, as $-\nabla \cdot \langle \mathbf{u}' T' \rangle$ (i.e., the eddy TFC) and $-\langle \mathbf{u} \rangle \cdot \nabla \langle T \rangle$ (i.e., the mean TFC), using the 8-year average from 1 January 1996 to 1 January 2004. The second expression assumes a nondivergent horizontal flow analogous to Isachsen et al. (2012). Note the temperature fluxes computed in Figures 7 and 8 consist of both rotational and divergent components. The heat budget of the basin is governed by the divergent heat flux; hence, the rotational component should be separated. This difficult task is alleviated by analyzing the heat flux divergences, since the rotational component vanishes (Isachsen et al., 2012). Figure 9a shows the depth-averaged eddy TFC distribution in the domain, with elevated values over the Lofoten Escarpment. Along the Slope Current, there is a persistent divergence of eddy fluxes along the 1,000-m isobath (blue colors in Figure 9a). A segment along the Lofoten Escarpment, along the 1,000-m isobath marked between the triangles in Figure 9a, is analyzed in detail. Averages of the mean and eddy TFC are computed along this segment for each depth level, to obtain the vertical distribution (Figure 9b). A similar calculation is also made over the LB (Figure 9c).

The vertical profiles show a divergence of eddy fluxes along the Lofoten Escarpment (Figure 9b), indicating heat extracted by the eddies shed from the 1,000-m isobath. The divergence has a maximum around a depth of 400 m. Furthermore, the eddy flux divergences dominate the convergence of the mean flow, implying the importance of the cooling of the Slope Current by eddy fluxes in this region, which may become a heat source for warming of colder water offshore, also possibly deep into the LB. This is supported by the vertical profiles obtained inside the central LB contour (Figure 9c). Even though the magnitudes are smaller than at the slope, the eddy fluxes show convergence around a depth of 700 m. This is consistent with Figure 8b and suggests that the eddies shed off the Slope Current to some extent propagate into the LB. Furthermore, the convergence of fluxes associated with the mean flow is larger than the convergence of eddy fluxes and dominates near the surface. This is consistent with the drifter observations and implies that the contribution of the slab of AW advection from the southern sector is important for the LB heat budget.

4. Conclusions

Compared to the Greenland Basin and the Norwegian Basin, the LB stands out with 3 to 12 times larger volume-integrated net heat transport and 3 to 6 times larger surface heat loss. The main contributors to the LB heat budget are the mean advective heat flow from the AW along the southern LB sector and the eddy fluxes from the Lofoten Escarpment in the east.

Our main findings are (1) the contribution of near-surface heat transport by the mean flow entering the LB from south is of significant importance; (2) the heat transport from the Lofoten Escarpment is dominated by eddy fluxes and enters the LB from the east; and (3) the eddy temperature flux divergence has a subsurface maximum that is not captured by the surface drifters.

The southeastern corner of the LB is an entry hot spot for surface drifters. However, most of these drifters stay inside the basin for a short period, and hence, the associated heat loss is limited. Drifters with long residence time inside the basin enter from south and, to some extent, from east. The Eulerian and Lagrangian analyses both suggest that eddies propagate westward into the LB. A comparison of vertical profiles of eddy TFCs from the slope region and from the central basin supports this link. The eddy fluxes cool the mean slope current, a process dominated at subsurface, and act as a heat source in the central basin. The heat transport by the mean flow enters the basin from the south in the upper water column and averaged over the central LB, the convergence of temperature fluxes associated with the mean flow is the largest at surface. This is consistent with our analyses of observed and synthetic surface drifters which revealed that these water masses often experience long residence time inside the basin to contribute substantially to the LB heat loss.

The subsurface processes are important in controlling the heat fluxes and the TFC, both in the basin and over the slope. Detailed subsurface Lagrangian observations are needed. Because of the deep mixed layer in the LB, the water parcels can experience a vertical exchange in addition to the lateral exchange. 3-D Lagrangian trajectories, computed from eddy-resolving numerical simulations as presented here but with better vertical and time resolution and realistic vertical velocity fields, could identify pathway of water parcels in the water column and merit further studies.

Acknowledgments
This study received funding from the Research Council of Norway, through the project *Water mass transformation processes and vortex dynamics in the Lofoten Basin in the Norwegian Sea (PROVOLO)*, project 250784. The surface drifters used in this study are obtained from the Global Drifter Program (http://www.aoml.noaa.gov/phod/gdp/index.php). The model and drifter simulations were performed on resources provided by UNINETT Sigma2—the National Infrastructure for High Performance Computing and Data Storage in Norway. The 4-km ROMS model fields and the synthetic drifters are archived, open-access, at the Norstore research data archive (https://archive.norstore.no/). The 800-m ROMS model fields are available at the Thredds Service at the Norwegian Meteorological Institute (https://thredds.met.no/). The authors thank Inga Koszalka and Pål Erik Isachsen for their help and support, Jonathan Lilly for discussions, and two anonymous reviewers and the editor Laurie Padman for their suggestions and comments which helped to improve the manuscript.

References

Andersson, M., Orvik, K. A., Lacasce, J. H., Koszalka, I., & Mauritzen, C. (2011). Variability of the Norwegian Atlantic Current and associated eddy field from surface drifters. *Journal of Geophysical Research*, *116*, C08032. https://doi.org/10.1029/2011JC007078

Bosse, A., Fer, I., Søiland, H., & Rossby, T. (2018). Atlantic water transformation along its poleward pathway across the Nordic Seas. *Journal of Geophysical Research: Oceans*, *123*, 6428–6448. https://doi.org/10.1029/2018JC014147

Davis, R. E. (1991). Observing the general circulation with floats. *Deep Sea Research Part A. Oceanographic Research Papers*, *38*, S531–S571. https://doi.org/10.1016/S0198-0149(12)80023-9

Fer, I., Bosse, A., Ferron, B., & Bouruet-Aubertot, P. (2018). The dissipation of kinetic energy in the Lofoten Basin Eddy. *Journal of Physical Oceanography*, *48*, 1299–1316. https://doi.org/10.1175/JPO-D-17-0244.1

Haidvogel, D. B., Arango, H., Budgell, W. P., Cornuelle, B. D., Curchitser, E., Di Lorenzo, E., et al. (2008). Ocean forecasting in terrain-following coordinates: Formulation and skill assessment of the Regional Ocean Modeling System. *Journal of Computational Physics*, *227*(7), 3595–3624. https://doi.org/10.1016/j.jcp.2007.06.016

Isachsen, P. E. (2015). Baroclinic instability and the mesoscale eddy field aorund the Lofoten Basin. *Journal of Geophysical Research: Oceans*, *120*, 2884–2903. https://doi.org/10.1002/2014JC010448-

Isachsen, P. E., Koszalka, I., & Lacasce, J. H. (2012). Observed and modeled surface eddy heat fluxes in the eastern Nordic Seas. *Journal of Geophysical Research*, *117*, C08020. https://doi.org/10.1029/2012JC007935

Isachsen, P. E., LaCasce, J. H., Mauritzen, C., & Häkkinen, S. (2003). Wind-driven variability of the large-scale recirculating flow in the Nordic Seas and Arctic Ocean. *Journal of Physical Oceanography*, *33*(12), 2534–2550. https://doi.org/10.1175/1520-0485(2003)033<2534:WVOTLR>2.0.CO;2

Ivanov, V., & Korablev, A. A. (1995). Formation and regeneration of the pycnocline lens in the Norwegian Sea. *Russian Meteorology and Hydrology*, *9*(9), 62–69.
Köhl, A. (2007). Generation and stability of a quasi-permanent vortex in the Lofoten Basin. *Journal of Physical Oceanography*, *37*(11), 2637–2651. https://doi.org/10.1175/2007JPO3694.1
Koszalka, I., LaCasce, J. H., Andersson, M., Orvik, K. A., & Mauritzen, C. (2011). Surface circulation in the Nordic Seas from clustered drifters. *Deep-Sea Research Part I: Oceanographic Research Papers*, *58*(4), 468–485. https://doi.org/10.1016/j.dsr.2011.01.007
Koszalka, I., LaCasce, J. H., & Mauritzen, C. (2012). In pursuit of anomalies—Analyzing the poleward transport of Atlantic Water with surface drifters. *Deep-Sea Research Part II: Topical Studies in Oceanography*, *85*, 96–108. https://doi.org/10.1016/j.dsr2.2012.07.035
Laurindo, L. C., Mariano, A. J., & Lumpkin, R. (2017). An improved near-surface velocity climatology for the global ocean from drifter observations. *Deep-Sea Research Part I: Oceanographic Research Papers*, *124*, 73–92. https://doi.org/10.1016/j.dsr.2017.04.009
Lee, T., Fukumori, I., & Tang, B. (2004). Notes and correspondence temperature advection: Internal versus external processes. *Journal of Physical Oceanography*, *34*, 1936–1944.
Lumpkin, R., Grodsky, S. A., Centurioni, L., Rio, M. H., Carton, J. A., & Lee, D. (2013). Removing spurious low-frequency variability in drifter velocities. *Journal of Atmospheric and Oceanic Technology*, *30*(2), 353–360. https://doi.org/10.1175/JTECH-D-12-00139.1
Lumpkin, R., Maximenko, N., & Pazos, M. (2012). Evaluating where and why drifters die. *Journal of Atmospheric and Oceanic Technology*, *29*(2), 300–308. https://doi.org/10.1175/JTECH-D-11-00100.1
Lumpkin, R., & Pazos, M. (2007). Measuring surface currents with Surface Velocity Program drifters: The instrument, its data, and some recent results. In *Lagrangian analysis and prediction of coastal and ocean dynamics* (pp. 39–67). Cambridge: Cambridge University Press. https://doi.org/10.1017/CBO9780511535901.003
MacLachlan, C., Arribas, A., Peterson, K. A., Maidens, A., Fereday, D., Scaife, A. A., et al. (2015). Global Seasonal forecast system version 5 (GloSea5): A high-resolution seasonal forecast system. *Quarterly Journal of the Royal Meteorological Society*, *141*(689), 1072–1084.
Nilsen, J. E. Ø., & Falck, E. (2006). Progress in oceanography variations of mixed layer properties in the Norwegian Sea for the period 1948–1999. *Progress in Oceanography*, *70*, 58–90. https://doi.org/10.1016/j.pocean.2006.03.014
Nøst, O. A., & Isachsen, P. (2003). The large-scale time-mean ocean circulation in the Nordic Seas and Arctic Ocean estimated from simplified dynamics. *Journal of Marine Research*, *61*(2), 175–210. https://doi.org/10.1357/002224003322005069
Orvik, K. A., & Niiler, P. (2002). Major pathways of Atlantic water in the northern North Atlantic and Nordic Seas toward Arctic. *Geophysical Research Letters*, *29*(19), 1896. https://doi.org/10.1029/2002GL015002
Peralta-Ferriz, C., & Woodgate, R. A. (2015). Seasonal and interannual variability of pan-Arctic surface mixed layer properties from 1979 to 2012 from hydrographic data, and the dominance of stratification for multiyear mixed layer depth shoaling. *Progress in Oceanography*, *134*, 19–53. https://doi.org/10.1016/j.pocean.2014.12.005
Poulain, P. M., Warn-Varnas, a., & Niiler, P. P. (1996). Near-surface circulation of the Nordic seas as measured by Lagrangian drifters. *Journal of Geophysical Research*, *101*, 18,237–18,258. https://doi.org/10.1029/96JC00506
Raj, R. P., Chafik, L., Nilsen, J. E. Ø., Eldevik, T., & Halo, I. (2015). The Lofoten Vortex of the Nordic Seas. *Deep-Sea Research Part I: Oceanographic Research Papers*, *96*, 1–14. https://doi.org/10.1016/j.dsr.2014.10.011
Raj, R., Johannesen, J., Eldevik, T., Nilsen, J., & Halo, I. (2016). Quantifying mesoscale eddies in the Lofoten Basin. *Journal of Geophysical Research: Oceans*, *121*, 4503–4521. https://doi.org/10.1002/2016JC011637
Richards, C. G., & Straneo, F. (2015). Observations of water mass transformation and eddies in the Lofoten Basin of the Nordic Seas. *Journal of Physical Oceanography*, *45*(6), 1735–1756. https://doi.org/10.1175/JPO-D-14-0238.1
Rossby, T., Ozhigin, V., Ivshin, V., & Bacon, S. (2009). An isopycnal view of the Nordic Seas hydrography with focus on properties of the Lofoten Basin. *Deep-Sea Research Part I: Oceanographic Research Papers*, *56*(11), 1955–1971. https://doi.org/10.1016/j.dsr.2009.07.005
Rossby, T., Prater, M. D., & Søiland, H. (2009). Pathways of inflow and dispersion of warm waters in the Nordic seas. *Journal of Geophysical Research*, *114*, C04011. https://doi.org/10.1029/2008JC005073
Rudels, B., & Quadfasel, D. (1991). Convection and deep water formation in the Arctic Ocean-Greenland Sea System. *Journal of Marine Systems*, *2*(3-4), 435–450. https://doi.org/10.1016/0924-7963(91)90045-V
Segtnan, O. H., Furevik, T., & Jenkins, A. D. (2011). Heat and freshwater budgets of the Nordic seas computed from atmospheric reanalysis and ocean observations. *Journal of Geophysical Research*, *116*, C11003. https://doi.org/10.1029/2011JC006939
Shchepetkin, A. F., & McWilliams, J. C. (2005). The Regional Oceanic Modeling System (ROMS): A split-explicit, free-surface, topography-following-coordinate oceanic model. *Ocean Modelling*, *9*(4), 347–404. https://doi.org/10.1016/j.ocemod.2004.08.002
Shchepetkin, A. F., & McWilliams, J. C. (2009). Correction and commentary for "Ocean forecasting in terrain-following coordinates: Formulation and skill assessment of the regional ocean modeling system" by Haidvogel et al., J. Comp. Phys. 227, pp. 3595-3624. *Journal of Computational Physics*, *228*(24), 8985–9000. https://doi.org/10.1016/j.jcp.2009.09.002
Søiland, H., & Rossby, T. (2013). On the structure of the Lofoten Basin eddy. *Journal of Geophysical Research: Oceans*, *118*, 4201–4212. https://doi.org/10.1002/jgrc.20301
Spall, M. A. (2010). Dynamics of downwelling in an eddy-resolving convective basin. *Journal of Physical Oceanography*, *40*(10), 2341–2347. https://doi.org/10.1175/2010JPO4465.1
Toole, J. M., Timmermans, M. L., Perovich, D. K., Krishfield, R. A., Proshutinsky, A., & Richter-Menge, J. A. (2010). Influences of the ocean surface mixed layer and thermohaline stratification on Arctic Sea ice in the central Canada Basin. *Journal of Geophysical Research*, *115*, C10018. https://doi.org/10.1029/2009JC005660
Trodahl, M., & Isachsen, P. E. (2018). Topographic influence on baroclinic instability and the mesoscale eddy field in the northern north atlantic ocean and the nordic seas. *Journal of Physical Oceanography*, *48*(11), 2593–2607. https://doi.org/10.1175/JPO-D-17-0220.1
Umlauf, L., & Burchard, H. (2003). A generic length-scale equation for geophysical turbulence models. *Journal of Marine Research*, *61*(2), 235–265.
Uppala, S. M., Kållberg, P. W., Simmons, A. J., Andrae, U., Bechtold, V. D. C., Fiorino, M., et al. (2005). The ERA-40 Re-analysis. *Quarterly Journal of the Royal Meteorological Society*, *131*(612), 2961–3012.
Volkov, D. L., Belonenko, T. V., & Foux, V. R. (2013). Puzzling over the dynamics of the Lofoten Basin—A sub-Arctic hot spot of ocean variability. *Geophysical Research Letters*, *40*, 738–743. https://doi.org/10.1002/grl.50126
Volkov, D. L., Kubryakov, A. A., & Lumpkin, R. (2015). Formation and variability of the Lofoten basin vortex in a high-resolution ocean model. *Deep-Sea Research Part I: Oceanographic Research Papers*, *105*, 142–157. https://doi.org/10.1016/j.dsr.2015.09.001
Warner, J. C., Sherwood, C. R., Arango, H. G., & Signell, R. P. (2005). Performance of four turbulence closure models implemented using a generic length scale method. *Ocean Modelling*, *8*(1-2), 81–113.
Yu, L. S., Bosse, A., Fer, I., Orvik, K. A., Bruvik, E. M., Hessevik, I., & Kvalsund, K. (2017). The Lofoten Basin eddy: Three years of evolution as observed by Seagliders. *Journal of Geophysical Research: Oceans*, *122*, 6814–6834. https://doi.org/10.1002/2017JC012982